euspen's 24th International Conference & Exhibition, Dublin, IE, June 2024
www.euspen.eu

Study of calibration technique for hybrid structured-light metrology system

Yongjia Xu[1,*], Feng Gao[1], Yanling Li[1,2] & Xiangqian Jiang[1]

[1]EPSRC Future Metrology Hub, University of Huddersfield, Huddersfield, HD1 3DH, UK
[2]School of Mechanical Engineering, Hebei University of Technology, Tianjin 300130, China

*Correspondence: Y.Xu2@hud.ac.uk; Tel.: +44-7510-953359

Abstract

Numerous structured surfaces with composite materials are widely applied in advanced manufacturing. Hybrid structured-light metrology system has been proposed for in-line form measuring of the structured surfaces with both reflective and diffuse characters. A hybrid structured-light metrology system contains a fringe projection profilometry (FPP) subsystem and a phase measuring deflectometry (PMD) subsystem. Each subsystem measures rough surfaces and specular surfaces based on structured-light projection and reflection principle, respectively. Accurate calibration of the system is a challenge and highly influences the data stitching accuracy of the subsystems. In this paper, calibration technique is studied for the hybrid structured-light system to achieve good measurement accuracy. Specific targets are designed and manufactured for the calibration. Novel calibration algorithms are studied based on the calibration targets. Details of the calibration procedure are presented and discussed. Experiments have been conducted and verified the effectiveness of the proposed calibration technique by measuring structured composite samples with a calibrated portable hybrid structured-light metrology prototype. Experimental results demonstrate that the proposed calibration technique can significantly improve the data fusion accuracy and the prototype can achieve good measurement accuracy based on the proposed calibration technique.

Keywords: Optical metrology; Three-dimensional measurement; Structured light technique; Structured composite surfaces; Calibration.

1. Introduction

In-line surface measurement is an important section but still a challenge for precision and ultra-precision machining. Current widely used surface metrology techniques, such as coordinate measuring machine and stylus profilometer are hardly applied in in-line metrology due to their disadvantages of low measurement speed and large volume. By contrast, structured-light metrology techniques, such as fringe projection profilometry (FPP) [1-3] and phase measuring deflectometry (PMD) [4-6] have obvious benefits in fast speed, simple system configuration, and light weight. They are hot-topics in in-line surface form measurements but still have limited measurement ability affected by the reflective properties of the tested surfaces' materials. FPP reconstructs a measured surface's form data based on the scattered structured-light patterns on the surface. Therefore, it can only measure rough surfaces. PMD measures based on structured-light reflection and is only good at measuring specular surfaces.

Hybrid structured-light technique [7-8] has been studied to increase the measurement ability of structured-light technique, which combining the advantages of FPP and PMD. FPP subsystem and PMD subsystem work independently. The reconstruction data from the subsystems can be fused together to generate a completed form of the measured surfaces. Thus, hybrid structured-light technique has obvious advantage in measuring more wider range of surfaces with different reflective characteristics. An accurate data fusion between the subsystems is essential to achieve high measurement accuracy of the hybrid structured-light technique. Martin et al. studied a method to calibrate the subsystems based on a special designed target for a good data fusion [9]. The designed target consists of several specular surfaces and rough surfaces and is difficult to be manufactured. In order to increase data fusion accuracy of the subsystems of hybrid structured-light technique, a flexible calibration technique is investigated based on calibration targets that can be easily manufactured. Details of the calibration algorithms and strategy are also presented.

2. Principle and method

2.1. Measurement principle and system

Figure 1 presents an illustration of a stereo-camera hybrid structured-light metrology system [9]. The system contains two cameras, a projector and a screen. The cameras and the screen form a stereo PMD system, which measures reflective surfaces. Vertical and horizontal phase measuring profilometry (PMP) patterns are generated by a computer, displayed on the screen, and captured by the cameras through the reflection of the measured surfaces. The measured surfaces' form data can be calculated based on the captured fringe patterns. One of the cameras and the projector generate a FPP system, which can measure the form of rough surfaces. PMP patterns generated by the computer are projected by the projector on the measured surface and captured by the camera. FPP reconstructs the 3D data of the measured surfaces based on the captured structured-light patterns. The reconstructed 3D data of PMD and FPP are fused to generate the final output.

In our proposed hybrid structured-light metrology system [9], a plate beam splitter (BS) is applied to fold the optical beam paths to decrease the system volume. Figure 2 illustrates an equivalent configuration of the system.

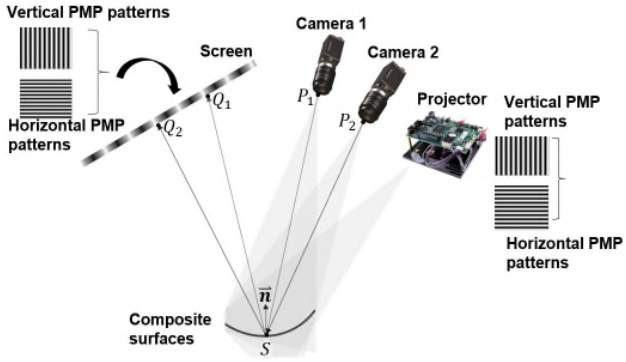

Figure 1. Illustration of the principle of the hybrid structured-light metrology technique

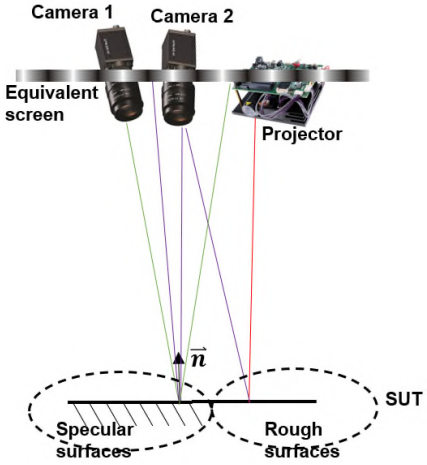

Figure 2. Illustration of configuration of a hybrid structured-light metrology system

2.2. Calibration method

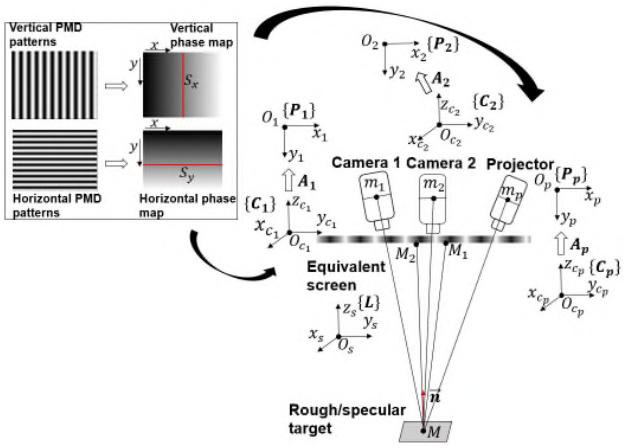

Figure 3. Illustration of the calibration of a hybrid structured-light metrology system

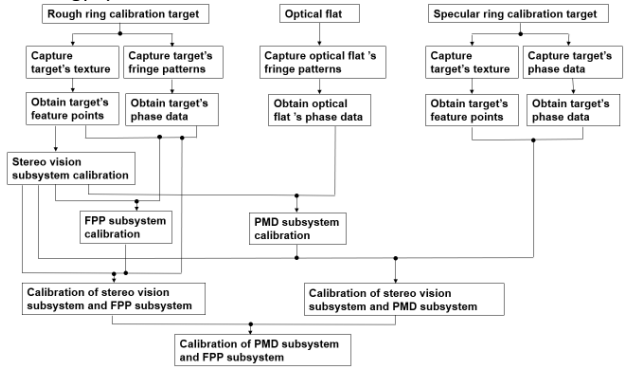

Figure 4. Diagram of the proposed hybrid structured-light metrology system calibration technique

Calibration is an essential process to obtain the imaging parameters of the hybrid structured-light metrology system for the surfaces' form reconstruction. This process also plays an important role in the data fusion between FPP subsystem and PMD subsystem. Figure 3 illustrates the purpose of the calibration process, which is to calculate the imaging parameters of the cameras (denoted as $\boldsymbol{A}_1$ and $\boldsymbol{A}_2$, respectively), the relationship between the cameras (using $\{\boldsymbol{C}_1\}$ and $\{\boldsymbol{C}_2\}$ to express the Camera 1 coordinate system and the Camera 2 coordinate system, respectively), the projector's imaging parameter (denoted as $\boldsymbol{A}_p$), the relationship between $\{\boldsymbol{C}_2\}$ and the projector coordinate system (expressed with $\{\boldsymbol{C}_p\}$), and the relationships between equivalent screen coordinate system (denoted as $\{\boldsymbol{L}\}$), $\{\boldsymbol{C}_1\}$, and $\{\boldsymbol{C}_2\}$. Figure 4 illustrates the strategy of the proposed calibration technique. A rough ring calibration target is placed at several arbitrary positions during the calibration process. The centre of the rings on target can be extracted through imaging processing. The ring centres are used as feature points to obtain $\boldsymbol{A}_1$, $\boldsymbol{A}_2$, and the relationship between $\{\boldsymbol{C}_1\}$ and $\{\boldsymbol{C}_2\}$, based on pin-hole model [10]. $\boldsymbol{A}_p$ and the relationship between $\{\boldsymbol{C}_2\}$ and $\{\boldsymbol{C}_p\}$ can be obtained by projecting fringe patterns on the rough ring target [11]. The relationships between $\{\boldsymbol{L}\}$, $\{\boldsymbol{C}_1\}$, and $\{\boldsymbol{C}_2\}$ can be calibrated based on the previous method [12] by using an optical flat. The ring centres of the rough calibration target can be reconstructed with two ways. One is the stereo cameras based on stereo vision algorithm [10]. Another is to calculate the 3D positions of the ring centres by using FPP. Using $\boldsymbol{F}$ to denote as the reconstructed 3D position of the ring centres by FPP, $\boldsymbol{S}$ express the corresponding reconstructed data by the stereo cameras. The relationship between the stereo vision system and the FPP system can be calculated based on Eq. (1).

$$\boldsymbol{S} = \boldsymbol{R}_{F\_S}\,\boldsymbol{F} + \boldsymbol{T}_{F\_S} \tag{1}$$

where $\boldsymbol{R}_{F\_S}$ and $\boldsymbol{T}_{F\_S}$ present the transformation relationship from the FPP system to the stereo vision system. A specular ring calibration target is used to obtain the relationship between stereo vision subsystem and PMD subsystem. A specular ring calibration target is applied to obtain the relationship between the stereo cameras system and the PMD system. The ring centres on the specular target can be reconstructed by the stereo cameras system and the PMD system, respectively. Denoting $\boldsymbol{S}$ as the reconstructed 3D data by the stereo cameras and $\boldsymbol{P}$ as the reconstructed data by the PMD, respectively. The relationship between the stereo cameras system and the PMD system can be obtained according to Eq. (2).

$$\boldsymbol{P} = \boldsymbol{R}_{S\_P}\,\boldsymbol{S} + \boldsymbol{T}_{S\_P} \tag{2}$$

where $\boldsymbol{R}_{S\_P}$ and $\boldsymbol{T}_{S\_P}$ are the transformation relationship from the stereo cameras system to the PMD system. Equation (3) can be used to conduct the relationship between the FPP system and the PMD system.

$$\begin{cases} \boldsymbol{R}_{F\_P} = \boldsymbol{R}_{S\_P}\boldsymbol{R}_{F\_S} \\ \boldsymbol{T}_{F\_P} = \boldsymbol{R}_{S\_P}\boldsymbol{T}_{F\_S} + \boldsymbol{T}_{S\_P} \end{cases} \tag{3}$$

where $\boldsymbol{R}_{F\_P}$ and $\boldsymbol{T}_{F\_P}$ represent the transformation from the FPP system to the PMD system. The reconstructed data from the FPP system and the PMD system can be fused accurately based on $\boldsymbol{R}_{F\_P}$ and $\boldsymbol{T}_{F\_P}$.

3. Experiment and results

A hybrid structured-light metrology prototype has been developed and calibrated with the proposed technique. Figure 5 shows pictures of the captured texture of the rough ring calibration target and the extracted feature points. Figures 5(a) and 4(b) are the texture captured by the Camera and the Camera 2, respectively. Figures 5(c) and 5(b) illustrate the extracted feature points on the texture pictures. Calibration results of the

optical parameters of the stereo cameras system is illustrated in Figure 6. Calibration error of the Camera 1 and the Camera 2 in stereo cameras system are demonstrated in Figures 6(a) and 6(b), respectively. The calibration error of the stereo cameras system is within ± 1 pixel. Figure 7 displays pictures of the calculated phase data of the optical flat. Figures 7(a) and 7(b) are the phase data obtained by the Camera 1 in horizontal and in vertical, respectively. Figures 7(c) and 7(d) are the phase data calculated by the Camera 2 in horizontal and in vertical, respectively. Figure 8 illustrates calibration results of the PMD system. Figures 8(a) and 8(b) demonstrate the calibration error of the Camera 1 and the Camera 2 in PMD system, respectively. The calibration error of the PMD system is within ± 5 pixels. Figure 9 shows pictures of the phase data of the rough ring calibration target obtained from the FPP system. Figures 9(a) and 9(b) are the horizontal and vertical phase data obtained by the Camera 2, respectively. Calibration results of the FPP system is shown in Figure 10. Reprojection error of the Camera 1 and the Camera 2 in FPP system are illustrated in Figures 10(a) and 10(b), respectively. The calibration error of the FPP system is within ± 1 pixel. Figure 11 shows pictures of the obtained phase data of the specular ring calibration target. Figures 11(a) and 11(b) illustrate the horizontal and vertical phase data obtained by the Camera 1, respectively. Figures 11(c) and 11(d) demonstrate the horizontal and vertical phase data obtained by the Camera 2, respectively. Figure 12 displays pictures of the captured texture of the specular target and the extracted feature points. The texture captured by the Camera 1 and the Camera are shown in Figures 12(a) and 12(b). The extracted feature points of the texture pictures are illustrated in Figure 12(c) and 12(d). Figure 13 illustrates the calibration results the relationship between the subsystems. Figure 13(a) compares the reconstruction error between the stereo cameras system and the FPP system. Figure 13(b) is a comparison of the reconstruction error between the stereo cameras and the PMD system. The experimental results demonstrate that reconstruction error between the subsystems is decreased to around 50 μm by applying the proposed calibration technique. A structured composite workpiece has been measured by the hybrid structured-light metrology system calibrated by the proposed calibration technique. Figure 14(a) shows the picture of the measured workpiece. The reconstruction data of the workpiece is illustrated in Figure 14(b). The RMS of the reconstruction error of the rough surface and the specular surface are 24.8 μm and 0.4 μm, respectively.

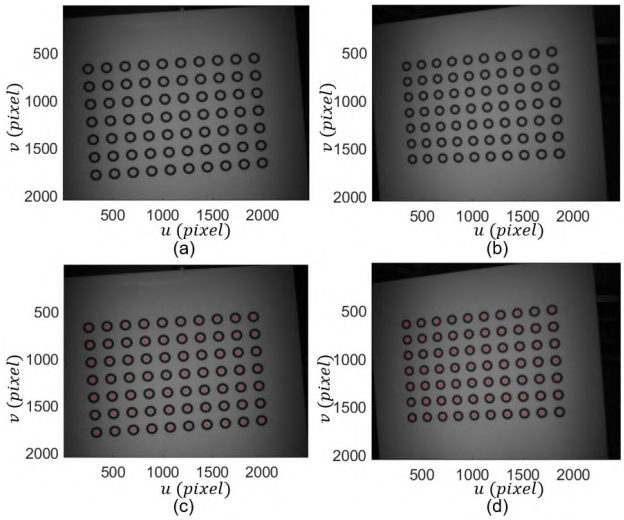

Figure 5. Pictures of the captured texture of the rough ring calibration target and the extracted feature points. (a) The texture captured by the Camera 1; (b) the texture captured by the Camera 2; (c) the extracted feature points of the Fig. 4(a); (d) the extracted feature points of the Fig. 4(b).

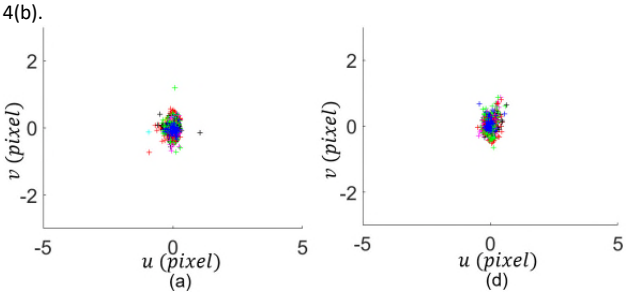

Figure 6. Calibration results of the optical parameters in the stereo cameras system. (a) Reprojection error of the Camera 1 in stereo vision system; (b) Reprojection error of the Camera 2 in stereo vision system

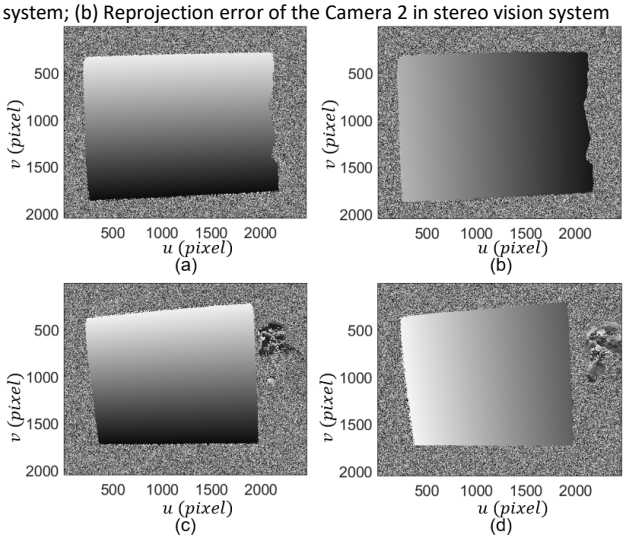

Figure 7. Pictures of the obtained phase data of the optical flat. (a) The phase data in horizontal obtained by the Camera 1; (b) phase data in vertical obtained by the Camera 1; (c) the phase data in horizontal obtained by the Camera 2; (d) phase data in vertical obtained by the Camera 2.

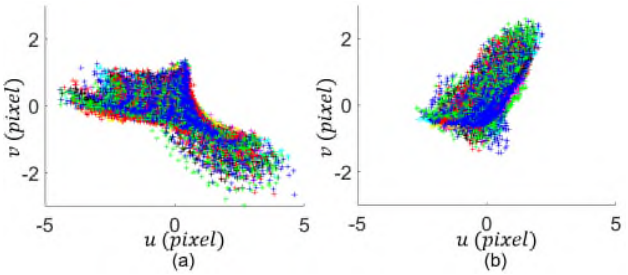

Figure 8. Calibration results of the optical parameters in the PMD system. (a) Reprojection error of the Camera 1 in PMD system; (b) Reprojection error of the Camera 2 in PMD system

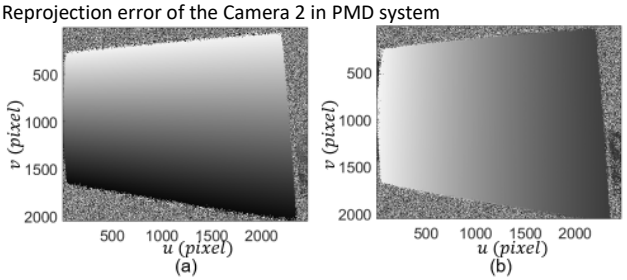

Figure 9. Pictures of the obtained phase data of the rough ring calibration target. (a) The phase data in horizontal obtained by the Camera 2; (b) phase data in vertical obtained by the Camera 2

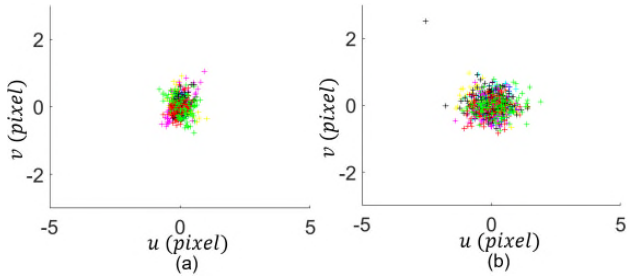

Figure 10. Calibration results of the optical parameters in the FPP system. (a) Reprojection error of the Camera 1 in FPP system; (b) Reprojection error of the Camera 2 in FPP system

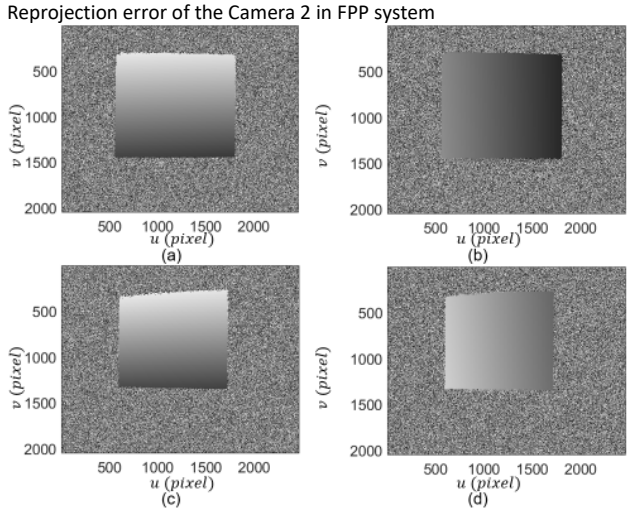

Figure 11. Pictures of the obtained phase data of the specular ring calibration target. (a) The phase data in horizontal obtained by the Camera 1; (b) phase data in vertical obtained by the Camera 1; (c) the phase data in horizontal obtained by the Camera 2; (d) phase data in vertical obtained by the Camera 2.

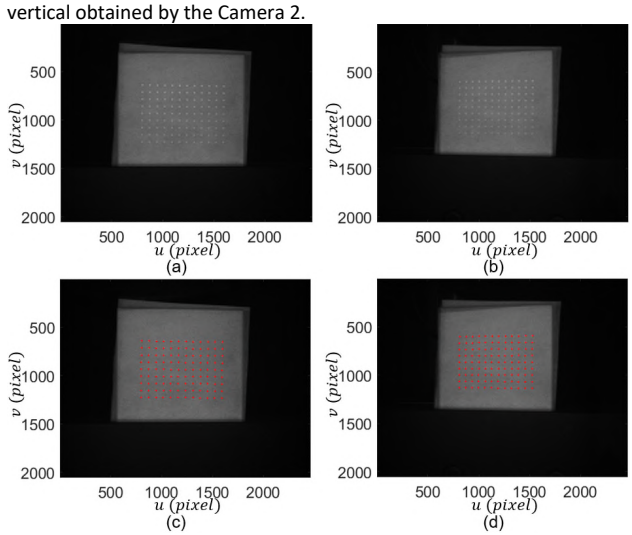

Figure 12. Pictures of the captured texture of the specular ring calibration target and the extracted feature points. (a) The texture captured by the Camera 1; (b) the texture captured by the Camera 2; (c) the extracted feature points of the Fig. 11(a); (d) the extracted feature points of the Fig. 11(b).

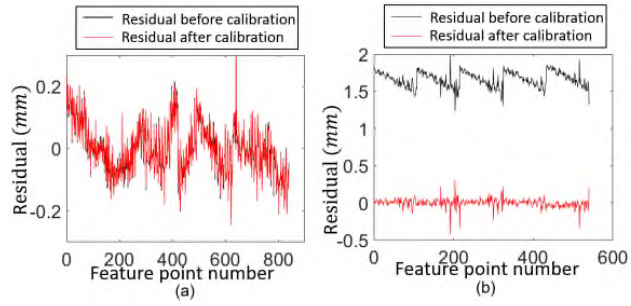

Figure 13. Calibration results the relationship between the subsystems. (a) a comparison of the reconstruction residual between the stereo vision subsystem and the FPP subsystem; (b) a comparison of the reconstruction residual between the stereo vision subsystem and the PMD subsystem

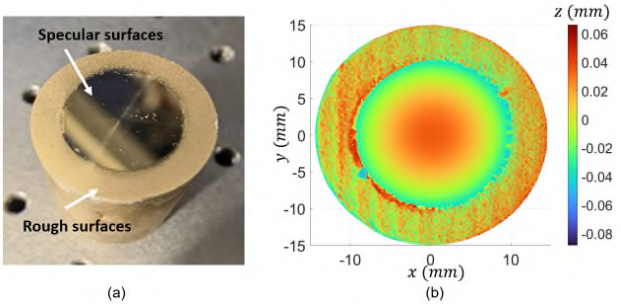

Figure 14. Measurement result of the structured composite workpiece. (a) A picture of the measured workpiece (b) the reconstruction data after data fusion of the subsystems

4. Conclusion

A calibration technique has been studied for hybrid structured-light system. Calibration targets, calibration algorithm, and strategy are described and discussed in this paper. The proposed calibration technique is easily conducted and has good calibration accuracy. More experiments will be conducted to test the calibration technique in the next step.

References

[1] Xu J and Zhang, S 2020 Opt. Lasers Eng. **135** 106193.

[2] Feng S, Zuo C, Zhang L, Tao T, Hu Y, Yin W, Qian J and Chen Q 2021 Opt. Lasers Eng. **143** 106622.

[3] Zhang Z, Xu Y and Liu Y. 2013 In2013 International Conference on Optical Instruments and Technology: Optoelectronic Measurement Technology and Systems **9046** 47-54.

[4] Xu Y, Gao F and Jiang X 2020 PhotoniX **1** 1-10.

[5] Huang L, Idir M, Zuo C and Asundi A 2018 Opt. Lasers Eng. **107** 247-257.

[6] Zhang Z, Chang C, Liu X, Li Z, Shi Y, Gao N and Meng Z 2021 Opt. Eng. **60** 020903.

[7] Liu X, Zhang Z, Gao N and Meng Z 3D 2020 Opt. Express **28**(19) 27561-27574.

[8] Breitbarth M, Kühmstedt P and Notni G 2009 In Optical Measurement Systems for Industrial Inspection **7389** 91-98.

[9] Xu Y, Gao F, Yanling L, Wenbin Z, Yang Y, Duo L and Jiang X 2024 Int. J. Extreme Manuf. Submitted.

[10] Zhang Z 2000 IEEE T. Pattern Anal. **22**(11) 1330-1334.

[11] Zhang S and Huang P S 2006 Opt. Eng. **45**(8) 083601-083601.

[12] Xu Y, Gao F, Zhang Z and Jiang X 2018 Opt. Lasers Eng. **106** 111-118.